ACS APPLIED POLYMER MATERIALS

pubs.acs.org/acsapm Article

Calcium Sulfate Formation on Different Zwitterionic Amphiphilic Copolymer Substrates for Salt Water Treatment

Meng Wang, Hoang Nguyen, Samuel J. Lounder, Ayse Asatekin, and Debora F. Rodrigues*

Cite This: ACS Appl. Polym. Mater. 2022, 4, 7090−7101 Read Online

ACCESS | Metrics & More | Article Recommendations | Supporting Information

ABSTRACT: Zwitterionic (ZI) polymers are a promising class of fouling-resistant and antiscaling coating materials. However, their mineral scaling prevention mechanism is still not well understood, which hampers the applications of ZI polymers. To fill this knowledge gap, we investigated the scaling mechanisms of different types of ZI amphiphilic copolymers (ZACs) synthesized from diverse combinations of zwitterion monomers and hydrophobic monomers using free-radical polymerization (FRP). The selected ZACs included poly(trifluoroethyl methacrylate-*random*-sulfobetaine methacrylate) (PTFEMA-*r*-SBMA, shortened as PT:SBMA), poly(trifluoroethyl methacrylate-*random*-2-methacryloyloxyethyl phosphorylcholine) (PTFEMA-*r*-MPC, shortened as PT:MPC), poly(methyl methacrylate-*random*-sulfobetaine methacrylate) (PMMA-*r*-SBMA, shortened as PM:SBMA), and poly(methyl methacrylate-*random*-2-methacryloyloxyethyl phosphorylcholine) (PMMA-*r*-MPC, shortened as PM:MPC). Coatings of these polymers were tested for calcium sulfate ($CaSO_4$) scaling in simulated brackish water solutions with different saturation indices, defined as the logarithm of the actual dissolved ion product (Q, i.e., calcium and sulfate ions) normalized by the solubility constant of gypsum (K_{sp}). These experimental results indicated that at high saturation indices (SI), the scaling deposition on ZAC coatings mainly depended on the surface energy. Therefore, PT:SBMA coatings, which had the lowest surface energy, exhibited better-scaling resistance. At lower SI, the hydrophilicity of the ZAC coatings was the dominant factor. Since ZAC coatings containing MPC have higher surface hydrophilicity, they might have a relatively slower scale-forming ion adsorption rate compared to SBMA containing ZACs, thus not markedly enriching the scale-forming ion near MPC coating surfaces and hence inhibiting heterogeneous $CaSO_4$ precipitates. The results demonstrated that the selection of ZAC coatings should consider the feed water chemistry and focus on the optimal prevention of scaling in addition to organic fouling.

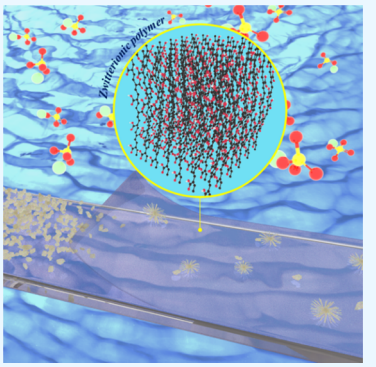

KEYWORDS: *zwitterionic amphiphilic copolymers (ZACs), coating, calcium sulfate ($CaSO_4$) scaling, scaling-resistant, saturation indices*

1. INTRODUCTION

The formation of mineral scale is a bottleneck in various industries, including water treatment,[1] oil and gas production,[2] power generation plants,[3] and food processing.[4] Scale accumulation might lead to the blockage of membrane modules or the clogging of pipelines and valves, thus shortening the equipment life span. This can increase maintenance costs and worsen production efficiency.[1] Inorganic scales (e.g., gypsum and calcite) are formed once the concentration of inorganic ionic species in the natural water exceeds their corresponding solubility limits.[1] As a consequence, mineral scaling usually occurs on the substrate−liquid interface through directly surface-induced heterogeneous nucleation and growth or the deposition of the crystals from the bulk solution where the crystals are initiated via homogeneous nucleation and growth.[5]

Inorganic ionic species, including calcium, sulfate, carbonate, and phosphate, are abundantly present in natural water (e.g., brackish water, seawater), thus causing frequent scaling with gypsum, calcite, calcium phosphate, and others. Most of these scales can be removed by controlling the pH of the feed water as a pretreatment step, except for gypsum ($CaSO_4{\cdot}2H_2O$), which is not sensitive to pH as the others.[6] Gypsum scales typically have very low solubility and strong adhesion, which make their removal from the surface challenging.[7] To prevent scale formation, both operational and material strategies, including antiscalant additives and the application of scale-resistant surface coatings, have been enforced in the practice, with the former being widely accepted in the industry.[8−14] Nevertheless, antiscalants only delay the onset of precipitation in the feed solution and might not inhibit the nucleation and growth of the scale on the substrate−liquid interfaces.[9,10] Furthermore, the removal of antiscalants increases energy consumption and operational cost and also poses a threat to the environment.[8,15] On the other hand, the development of

Received: June 14, 2022
Accepted: September 12, 2022
Published: September 29, 2022

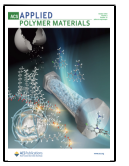

scale-resistant coatings can enable us to avoid those restrictions at a much lower cost.[11,12,16] For example, superhydrophilic or hydrophobic coatings have been shown to affect the nucleation energy barrier, resulting in attenuation of the nucleation and deposition of minerals on the surface.[13−15] To date, the underlying scaling mechanisms on different organic coatings have been extensively studied to demonstrate that the surface functional groups,[17,18] the surface hydrophilicity,[19,20] and ion adsorption[21,22] can control the formation of mineral scaling. Moreover, the inertia of hydrophilic and neutrally charged surface coatings to inorganic scalants has been proposed.[23] Therefore, numerous hydrophilic coating materials for the membrane and other surfaces including graphene oxide (GO),[14] poly(ethylene glycol) (PEG),[24] and zwitterionic (ZI) polymers[23] have been developed. ZI polymers possess equal numbers of positively and negatively charged zwitterionic functional groups, which make them known for excellent hydration capacities and antifouling properties.[25,26] In addition to the hydrophilicity, ZI polymers also have other properties (i.e., neutral charge), which might contribute to the scaling-resistant performance. However, how the properties of ZI polymers would affect mineral scaling has not been explored thoroughly.

In the study of Jaramillo et al., poly(sulfobetaine methacrylate) (pSBMA) brushes were grafted on reverse osmosis (RO) membrane surfaces, which have been shown to be effective for curtailing scaling. These zwitterion-grafted membrane surfaces were shown to exhibit increasing hydrophilicity, thus causing a delay in gypsum nucleation and adsorption.[23] However, this study only revealed the scaling mechanisms from the thermodynamic perspective, while the interactions between crystal-forming ions and ZI moieties are still unclear. Other studies of how ZI materials interact with natural water sources typically focused on organic fouling rather than scaling. ZACs, which are made of a hydrophobic monomer (e.g., trifluoroethyl methacrylate, TFEMA) with a ZI monomer, have been studied as membrane coatings or selective layers. These ZACs exhibit size-selective permeation of solutes and are extremely resistant to fouling by a broad range of wastewater sources containing oil emulsions, common foulants in surface water and municipal wastewater, and when treating textile wastewater. This is believed to be due to the excellent self-association and hydration capabilities of ZI monomers in the copolymer structure.[27,28] Dudchenko et al. investigated the effects of chemically heterogeneous ZAC coatings on organic foulant adsorption by changing the weight percent of the ZI monomer in the copolymer structure. This work indicated that surface hydrophilicity is not sufficient for explaining the foulant adsorption on ZAC coatings, and the heterogeneity of surfaces due to the microphase separation of ZACs likely contributes to their interaction with organic foulants.[29] These studies demonstrate the potential of ZAC coatings for organic fouling resistance. ZACs also exhibit a self-assembled, chemically heterogeneous structure that may further influence calcium sulfate scaling formation. The effects of these features are still not fully understood.

Previous studies indicate that ZACs are extremely resistant to organic fouling by a variety of macromolecular solutes as well as oil when they were used not only as membrane-selective layers but also as electrospun fibers[30] and coatings.[29] While their unique hydration capabilities imply the likelihood that they can be scaling-resistant, systematic studies on how ZAC coatings resist scaling are needed. In the present study, we studied $CaSO_4$ scaling on different types of ZAC coatings with two specific objectives: (1) to elucidate the effects of the surface chemistry (i.e., the surface hydrophilicity, surface roughness) of ZAC coatings on $CaSO_4$ precipitation and (2) to determine the interactions among ZAC coatings, crystal-forming ions, and precipitates. The ZACs in our study were synthesized by copolymerizing sulfobetaine-based monomers (i.e., SBMA) and phosphorylcholine-based monomers (i.e., MPC), the ZI monomers of the two ZACs that exhibited excellent antifouling properties with organic feeds as we discussed before.[27,28] They are also different in hydration capability, which might influence the overall scaling-resistant performance and thus enable better visualization of the mineralization mechanism. Batch $CaSO_4$ scaling tests on various types of ZAC coatings that combine two types of hydrophobic monomers with two types of ZI monomers were conducted in aqueous solutions of various supersaturation levels. Detailed surface coating characterizations were done to determine the dominant scaling mechanisms.

2. MATERIALS AND METHODS

2.1. Materials. 4-Methoxy phenol (MEHQ, 95%), α,α'-azoisobutyronitrile (AIBN, 98%), activated aluminum oxide (basic, Brockmann I, standard grade), methyl methacrylate (MMA), 2-methacryloyloxyethyl phosphorylcholine (MPC), and sulfobetaine methacrylate (SBMA, 95%) were purchased from Sigma-Aldrich. Denatured alcohol, dimethyl sulfoxide (DMSO, ACS certified), isopropyl alcohol (IPA, 99.5%), and trifluoroethanol (TFE, ≥99.0%, used in synthesis and purification) were purchased from Fisher Scientific. Hexane (≥98.5% *n*-hexane and mixed C6-isomers) and 2,2,2-trifluoroethyl methacrylate (TFEMA, 99%) were purchased from VWR and Scientific Polymer Products Inc., respectively. d_6-DMSO (99.5%) was obtained from Cambridge Isotope Laboratories Inc. Concentrated sulfuric acid (H_2SO_4, 98%), 2,2,2-trifluoroethanol (TFE, used for coatings), hydrogen peroxide (H_2O_2, 30%), and sodium dodecyl sulfate (SDS) were purchased from Sigma-Aldrich. Sodium sulfate anhydrous (Na_2SO_4), calcium chloride dehydrate ($CaCl_2{\cdot}2H_2O$), and glass slides (Superfrost Plus, >72.2 wt % SiO_2) were purchased from Fisher Scientific. All reagents were used as received except for TFEMA and MAA that require removing the inhibitor with a basic alumina column. Compressed nitrogen (ultrahigh purity, used for synthesis) was purchased from Airgas.

2.2. Synthesis and Selection of ZACs. Different types of ZACs were synthesized using methods described in the previous work.[27,28] Zwitterionic monomers (i.e., SBMA and MPC) and hydrophobic monomers (i.e., 2,2,2-trifluoroethyl methacrylate (TFEMA, abbreviated in copolymer structures as PT), methyl methacrylate (MMA, abbreviated in copolymer structures as PM)) were randomly copolymerized using free-radical polymerization (FRP) method to form a random/statistical copolymer. Four types of ZACs including poly(trifluoroethyl methacrylate)-*r*-sulfobetaine methacrylate (PT:SBMA, 36 wt % SBMA), poly(trifluoroethyl methacrylate)-*r*-methacryloxyphosphorylcholine (PT:MPC, 34 wt % MPC), poly(methyl methacrylate)-*r*-sulfobetaine methacrylate (PM:SBMA, 40 wt % SBMA), and poly(methyl methacrylate)-*r*- methacryloxyphosphorylcholine (PM:MPC, 34 wt % MPC) have been synthesized. The method for obtaining accurate compositions of these copolymers using ^{1}H NMR can be found in previous publications.[27,28] Detailed synthesis procedures, chemical structures, and ^{1}H NMR spectra of ZACs are presented in Text S1 and Figures S1 and S2, respectively. As mentioned before, ZACs with the highest organic fouling resistance were PT:SBMA and PT:MPC whose chemical structures may imply that they can be scaling-resistant. Therefore, PT:SBMA and PT:MPC were used to fabricate ZAC coatings. Also, the effect of the hydrophobic unit on scaling was also investigated by changing the hydrophobic units from TFEMA to MMA (Figure S1).

https://doi.org/10.1021/acsapm.2c01014
ACS Appl. Polym. Mater. 2022, 4, 7090−7101

2.3. Substrate Preparation. Glass slides (around 15 mm × 15 mm × 1 mm) were cleaned with acetone and then a mixture of sulfuric acid (98%) and Nochromix to remove all traces of organic residues.[31,32] Next, the substrates were flushed with copious deionized (DI) water and dried using argon gas. Afterward, an acid-based piranha solution (3:1 H_2SO_4/H_2O_2) was prepared to treat the glass slides for 30 min and washed using the same procedure mentioned earlier. The purpose of the acid bath was to improve the bonding strength between ZACs and substrates due to the chemical etching and the formation of hydroxyl functional groups on the glass surfaces after cleaning treatment.

These selected ZACs were first dissolved in 2,2,2-trifluoroethanol (TFE) at 50 °C to make a 3 wt % solution. The copolymer solutions were filtered using a 0.45 μm syringe filter made of polytetrafluoroethylene (PTFE, Wheaton Co.) and degassed by heating to 50 °C in a sealed vial for 1 h until no visible gas bubbles were observed. After that, a 100 μL solution was withdrawn and spin-coated on the glass slides. The samples were spun at 3000 rpm for 1 min and annealed in the vacuum oven under 80 °C for 30 min to form the required ZAC coatings for subsequent experiments. The successful coating was determined by subsequent surface characterizations.

2.4. Characterizations of Zwitterionic Amphiphilic Random Copolymer Coatings. *2.4.1. Attenuated Total Reflection Fourier-Transform Infrared Spectroscopy (ATR-FTIR).* To confirm that ZACs were successfully coated on the glass, attenuated total reflection Fourier-transform infrared spectroscopy (ATR-FTIR, Digital lab FTS-700) measurements were performed to obtain the IR spectrum of the glass slides before and after spin coating. The spectra for each sample were collected in an absorbance mode within the range of 650−4000 cm^{-1}. Meanwhile, 96 scans at a resolution of 4 cm^{-1} were taken during the measurement.[14]

2.4.2. Surface Hydrophilicity and Surface Energy. The contact angles between different types of liquid droplets including water (polar liquid), ethylene glycol (polar liquid), and diiodomethane (nonpolar liquid) and ZAC coatings were characterized using a data physics OCA 15EC goniometer to calculate the surface energy of ZAC coatings.[33] Briefly, 5 μL of selected liquid droplets was dispensed on bare and ZAC-coated glass slides. After 5 s, the contact angle between the droplet and the substrate was captured and measured. The average contact angle was reported based on five measurements at various sections of ZAC-coated surfaces. The detailed calculation protocols for surface tension can be seen in the Supporting Information (Text S2).

2.4.3. Captive Air Bubble Measurements. In addition to the sessile drop method, the surface hydrophilicity in the hydrated condition was characterized using the captive air bubble method. Using this method, the influence of swelling or pores on the measurements can be avoided, as described in previous publications.[27] Specifically, ZAC coatings were required to immerse in DI water at least 4 h before the measurements. Then, they were fixed on the holder with the coated side facing down. After that, both the holder and the mounted slides were immersed in a rectangular chamber prefilled with DI water. Next, a 5 μL air bubble was dispensed on the ZAC coating surfaces using a syringe with a bent U-shaped needle tip. The volume of air used was relatively large to make the edges of the bubble clear.[34] In the final step, the air-in-water contact angle was captured using a live camera. The measurement was done in triplicate at different spots on the coated surfaces. The average contact angles and their standard deviations were reported.

2.4.4. Surface Roughness. Tapping mode atomic force microscopy (AFM, Innova, Bruke Inc.) was performed to obtain the surface roughness of ZAC coatings, in which the coated slides were placed on the carbon disk prior to the measurement. During the measurement, an area of 10 μm by 10 μm for each sample was scanned at a scanning rate of 0.5 Hz. Triplicate measurements for each coating were done, and the surface roughness was calculated based on the collected height images using the Nano-scope Analysis program, version 1.5.

2.4.5. Surface ζ Potential. An electrokinetic analyzer (Anton Paar, SurPASS) was employed to characterize the surface charge of ZAC coatings referencing the previously reported protocols.[35,36] First, two 1 cm × 2 cm coated substrates with the same coating were clamped between the cells. A 10 mM sodium chloride, as the background electrolyte, was infused into the instrument, which should be rinsed ahead twice with DI water for 60 s. During the measurement, dosing 0.1 M hydrochloric acid (HCl) or 0.1 M sodium hydroxide (NaOH) was to control the pH of the electrolyte solution range from 3 to 10. Triplicate surface ζ potential values were measured for each sample under different pH conditions. The average value and the standard deviation were calculated.

2.5. Batch Calcium Sulfate Scaling Tests under Quiescent Conditions. *2.5.1. Batch Calcium Sulfate Scaling Tests.* The mineral solutions were prepared based on the solution compositions listed in Table 1, which was designed to simulate brackish water.[37,38]

Table 1. Initial Compositions of the Mineral Solution for Scaling Tests[a]

condition no.	$CaCl_2$ (mM)	Na_2SO_4 (mM)	ionic strength (mM)	pH	bulk SI_{gyp}	reaction time (h)
1	30	30	135	5.6	0.07	8
2	50	50	218	5.6	0.32	3

[a]Note: SI refers to saturation index, which is defined by the formula $SI = \log_{10}(Q/K_{sp})$.[21,39] Q represents the actual product of the dissolved composition, and K_{sp} refers to the equilibrium constant of gypsum, which is based on the thermodynamic database from the software mentioned above.

The initial solutions' saturation indices (SI) with respect to gypsum (SI_{gyp}) were predetermined using SPEC-E8 in Geochemist's Workbench software (GWB, 11.0. 6, Aqueous Solution LLC).[21,39] In solution 1, the solubility of gypsum in the initial solution was slightly saturated (SI_{gyp} = 0.07; Table 1). Under this condition, heterogeneous precipitation mainly occurred on the coatings. For solution 2, the saturation level with respect to the gypsum of the initial solution (SI_{gyp} = 0.32; Table 1) was increased to oversaturate. After mixing the calcium chloride and sodium sulfate, the homogeneous nucleation of $CaSO_4$ particles in the bulk solution occurred within a short time under such conditions, thus finally leading to the deposition of $CaSO_4$ crystals on the substrate dominantly.[7] After soaking bare and ZAC-coated glass slides into the simulated solutions, batch reaction tests were conducted under stirring. To ensure adequate precipitation for quantification analyses, the reaction time for scaling tests under condition 1 (SI_{gyp} = 0.07) and condition 2 (SI_{gyp} = 0.32) was controlled for 8 and 3 h, respectively. The samples were collected for the subsequent characterizations after the reaction.

2.5.2. Characterizations of Calcium Sulfate Precipitates on ZAC Coatings. Two groups of the $CaSO_4$ scaling tests were conducted for scanning electron microscopy (SEM) observation and precipitate quantification experiments, respectively. For SEM, the samples after scaling were scanned under SEM (Nova NanoSEM 230) with an accelerating voltage of 10 kV to image the precipitate morphologies on bare glass slides and ZAC coatings.[14] For the precipitate quantification tests, the substrates after scaling were dissolved to quantify the amounts of precipitates on bare and ZAC-coated slides with atomic absorption spectrometry (AAS, AAnalyst 200, and PerkinElmer Inc.). To perform AAS analysis, the ZAC-coated glass slides were retrieved from the simulated solution and rinsed with DI water to remove any unbounded ion residues. After drying using argon gas, the substrates were soaked in 6 mL of hydrochloric (HCl, 0.5 (v/v %)) acid overnight to dissolve completely the precipitates formed on the substrates.[40] Then, the concentration of calcium (Ca) in the acidized solution was quantified by AAS for each sample. Based on the concentration of Ca, the mass of Ca in the dissolution solution was also calculated. Bare glass slides were also subjected to the same experiment as a control group. Ten replicate experiments were done for each condition. The average concentration, average mass of Ca in the acidized solution, and their standard deviation were reported. In addition, Student's *t*-tests were done to evaluate the statistical

https://doi.org/10.1021/acsapm.2c01014
ACS Appl. Polym. Mater. 2022, 4, 7090−7101

Table 2. Characteristics of Random Zwitterionic Amphiphilic Copolymers[a]

Copolymer name	Chemical structure	Zwitterion content percentage in ZAC (%)	Hydrodynamic size (nm)	Molecular weight (g/mol)	Solubility
PTFEMA-*r*-SBMA (PT:SBMA)	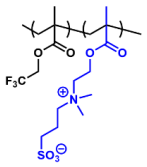	36	36.5±1.4	3.0×10^6	Not soluble in water, ethanol, and methanol
PMMA-*r*-SBMA (PM:SBMA)	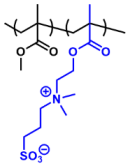	40	36.0±1.2	2.92×10^6	Soluble in TFE, dimethyl sulfoxide solvent
PTFEMA-*r*-MPC (PT:MPC)	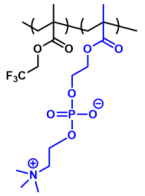	34	25.9±2.2	1.36×10^6	Not soluble in water
PMMA-*r*-MPC (PM:MPC)	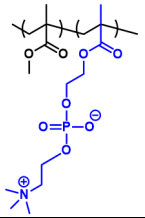	34	35.14±0.6	2.75×10^6	Soluble in TFE, dimethyl sulfoxide. ethanol, and methanol

[a]Note: hydrodynamic size and molecular weight were measured using the method described in our prior publications.[27,28]

difference in the precipitated amount generated on different ZAC coatings.

2.6. Calcium and Sulfate Ion Adsorption. Quartz crystal microbalance with dissipation (QCM-D) tests were performed to investigate the interactions between scale-forming ions and ZAC coatings. Each QCM-D experiment was conducted with a new silica sensor (QSX 303, silicon dioxide (SiO_2), Biolin Scientific) prepared as follows: first, a new sensor was treated for 10 min using UV/ozone cleaner and then was soaked in a 2% SDS solution for half an hour. After that, DI water was used to thoroughly flush the sensor and dried with soft steam of argon gas before UV/ozone treatment for another 20 min.[7] Next, the QCM crystal was mounted on the spin coater and spun at 3000 rpm for 2 min after the addition of 2−3 droplets of ZAC solutions and annealed in the oven at 80 °C for 30 min.[41] To verify the successful spin coating of polymer films, AFM and the sessile drop method were used to characterize the surface morphology and hydrophilicity of ZAC coatings (Figures S3 and S4), and the thickness of the ZAC film was around 100−200 nm (Figure S5).

Prior to pumping into the flow chamber, the test solutions were filtered and degassed using a 0.22 μm vacuum filter and a sonication bath sequentially. The procedure for solution infusion was first to pump ultrapure water to establish a stable baseline with a flow rate of 200 μL/min at 23 °C. Then, 30 mM $CaCl_2$ and Na_2SO_4 as sources for calcium and sulfate ion adsorption, respectively, were separately injected into the flow module with the same flow rate (QSense, E4). Once the change of the frequency reached equilibrium, the flow of the salt solution was stopped. After that, ultrapure water was fed again for ion desorption from ZAC coatings. Duplicate experiments of calcium or sulfate adsorption were carried out for each type of ZAC coatings. During the measurements, the changes of both frequency (Δf) and dissipation (ΔD) at varied overtones (1, 3, 5, 7, 9, 11, and 13) were monitored. And the third overtone was reported, as shown in Figures 5, S6, and S7.

After the QCM-D investigation, Δf and ΔD caused by the ion adsorption were processed using the QTools program (Biolin Scientific AB, v.3.0) based on the Sauerbrey model and Kelvin−Voigt model. If the values of $|-\Delta D/(\Delta f/n)|$ were greater than 4×10^{-7}, the Voigt viscoelastic model that assumes a frequency is linearly dependent on the viscous modulus used to calculate the absorbed masses. Otherwise, the Sauerbrey model was adopted, as per the equation below[42,43]

$$\Delta m = -C\frac{1}{n}\Delta f \tag{1}$$

here, Δm (ng/cm^2) is referred to as the change of mass, Δf (Hz) is the change of resonance frequency, n is the overtone number, and C is the mass-sensitivity constant, 17.7 ng/cm^2.

3. RESULTS AND DISCUSSION

3.1. Characterization Results of Zwitterionic Amphiphilic Copolymer (ZAC) Coatings. In the present study, the scaling potential effect of hydrophobic groups and ZI group chemistry was investigated. For this reason, we synthesized four copolymers combining either a fluorinated hydrophobic monomer (TFEMA, shortened as PT in copolymer names) or methyl methacrylate (MMA, shortened as PM in copolymer

https://doi.org/10.1021/acsapm.2c01014
ACS Appl. Polym. Mater. 2022, 4, 7090−7101

names) with one of two monomers (SBMA or MPC). The resulting copolymers had similar zwitterionic monomer contents between 34 and 40 wt % (Table 2 and Figure S2). This range was previously identified to be effective as organic fouling-resistant membrane-selective layers without exhibiting solubility in water.

After the spin coating of those copolymers mentioned above, the ATR-FTIR spectra of PM:MPC, PM:SBMA, PT:SBMA, and PT:MPC were collected to confirm the presence of zwitterionic moieties, which are the sulfobetaine moieties belonging to SBMA monomers and the phosphonate moieties in MPC monomers.[44] As illustrated in Figure 1, the peaks of

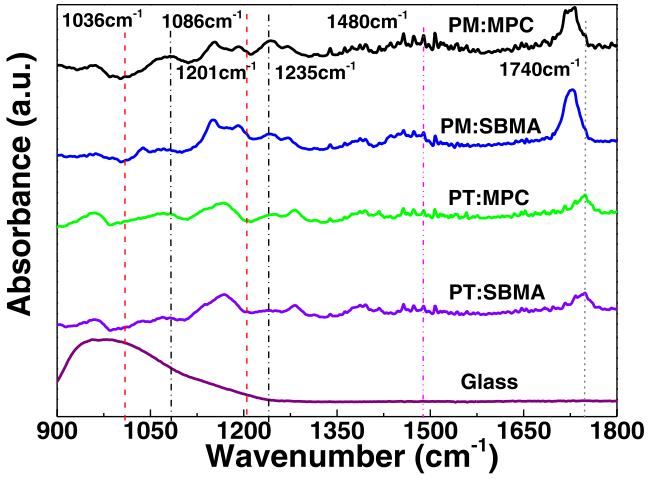

Figure 1. IR spectrum of glass slides and different types of ZAC coatings including PM:MPC, PM:SBMA, PT:MPC, and PT:SBMA. In the figure, the red dash-dot lines represent the sulfobetaine groups (SO_3^- around 1036 and 1201 cm^{-1}) in PT: SBMA and PM:SBMA. The black dashed lines represent the phosphonate functional groups ($-OPOCH_2-/-POCH_2-$) (around 1086 and 1235 cm^{-1}) in both PT:MPC and PM:MPC. The pink dash-dot line represents the quaternized ammonium functional groups ($N^+(CH_3)_3$, around 1480 cm^{-1}). And the gray dash-dot line shows the carbonyl bond (C═O) of the ester groups (around 1740 cm^{-1}).[27,28]

the sulfobetaine functional groups in PT:SBMA and PM:SBMA were observed at 1036 and 1201 cm^{-1}.[27] For both PT:MPC and PM:MPC, the peaks corresponding to the phosphonate functional groups ($OPOCH_2$, $POCH_2$) were shown at 1086 and 1235 cm^{-1}.[27] Also, the characteristic peaks of quaternized ammonium functional groups were found for all four types of ZI polymers at 1480 cm^{-1}.[27,28] The carbonyl bond (C═O) of the ester groups occurred at 1740 cm^{-1}, confirming the existence of hydrophobic units of TFEMA and MMA.[28] All of the above-mentioned peaks appear together with the characteristic peaks of glass (949 cm^{-1}), indicating that ZACs were coated on the glass slides successfully.

In Figure 2, the water contact angles measured in dry conditions of all ZAC coatings were greater than 90° with no significant statistical difference. This is in line with the prior study by Bengani−Lutz,[27,28] where the hydrophobic ZAC surfaces were attributed to the reorganization of zwitterion functional groups to minimize the surface energy, thus leaving the hydrophobic units of ZACs exposed to the air. However, the captive bubble contact angles measured under the hydrated condition apparently decreased compared to those water contact angles, confirming the excellent hydration capabilities of the zwitterionic functional groups due to the binding to

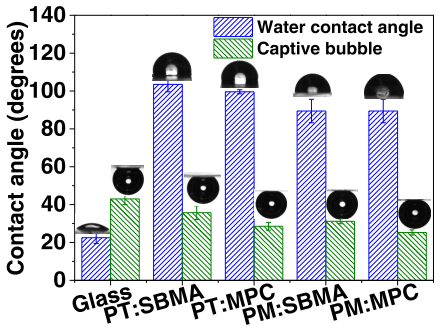

Figure 2. Water contact angles and the captive bubble contact angles of different substrates including glass slides, PT:SBMA, PT:MPC, PM:SBMA, and PM:MPC.

water molecules via the electrostatic interactions. ZAC coatings containing the MPC monomer (i.e., PT:MPC, PM:MPC) presented a relatively lower air-in-water contact angle than those coating containing the SBMA monomer (i.e., PT:SBMA, PM:SBMA), which indicated that the phosphorylcholine (MPC) was more hydrophilic than the sulfobetaine (SBMA).[27] This difference in the surface hydrophilicity is because the charge density between cation and anion moieties of MPC were less than those of SBMA.[43] In addition, the captive air bubble contact angles of ZAC coatings (i.e., PT:SBMA, PM:SBMA) containing the same zwitterion monomer but with different hydrophobic monomer exhibited no obvious statistical difference, suggesting that the surface wetting ability of ZAC coatings under the fully hydrated condition might be dominated by the zwitterionic content.

Previous studies revealed that surface hydrophilicity is related to structural (surface roughness) and molecular (surface charge) properties.[39] Surface roughness of different ZAC coatings was determined by AFM scanning measurements (Figure S4). As shown in Figure 3, there was no obvious

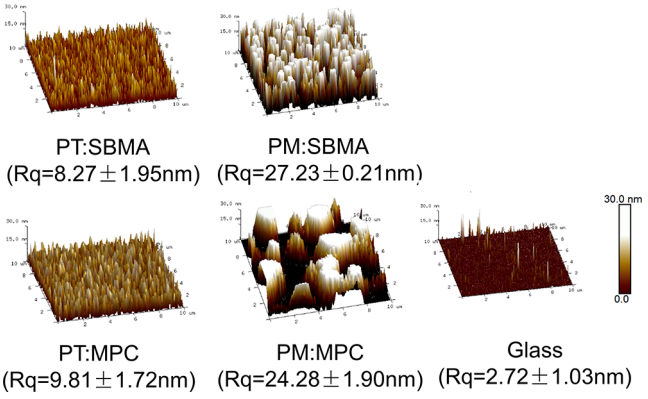

Figure 3. AFM images and average root-square-roughness of PT:SBMA, PT:MPC, PM:SBMA, PM:MPC, and control glass slides. The scan range is 10 μm × 10 μm.

statistical difference (Student's t-test: $p = 0.27 > 0.05$) in the average square-root-roughness between PT:SBMA and PT:MPC, whereas the surface of PM:SBMA coating was rougher than that of PM:MPC. Overall, the surfaces of ZAC coatings copolymerized from TFEMA (i.e., PT:SBMA, PT:MPC) were relatively smoother than those copolymerized from MMA (i.e., PM:MPC, PM:SBMA). This may arise from the differences in the viscosities of the polymer solutions. We

https://doi.org/10.1021/acsapm.2c01014
ACS Appl. Polym. Mater. 2022, 4, 7090−7101

have also observed that humidity during the spin-coating process may also have affected surface roughness, likely due to water vapor uptake into the polymer solution.

Besides the surface roughness, the surface zeta potential of PT:MPC, PM:SBMA, and PM:MPC (Figure 4) exhibited negative charges over the whole range of pH from 3 to 10. The ζ potential values of the ZAC-coated glass substrates all followed the trend of the uncoated glass substrates, with a less negative surface charge for all coatings in comparison with the glass surface. ZACs do not have any weak acidic or basic groups in their structures. And they are expected to be neutral throughout the pH range shown. However, it is worth noting that these ZACs are permeable to water and ions.[27,28] As such, the ZAC films may act as thin, porous coatings, which decrease and shield the influence of the charged glass surface.

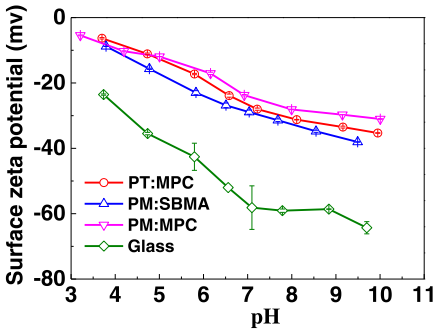

Figure 4. Surface zeta potential of glass, PT:MPC, PM:SBMA, and PM:MPC; note that the streaming potential measurements were under tangential crossflow at pressures around 10 psi for approximately 2 h. Under these experimental conditions, PT:SBMA coatings tended to detach from the substrate, so the surface ζ potential for PT:SBMA is not shown.

3.2. Interactions between Scale-Forming Ions and Different ZACs. As mentioned before, ion adsorption to surface functional groups played an important role in the surface heterogeneous crystallization, as heterogeneous precipitation initiates from the adsorption of scale-forming ions at the substrate−liquid interface.[32,45,46] The specific interaction between ions and surface functional groups could enrich scale-forming ions near the local substrate surface, promoting nucleation even under undersaturated conditions.[21] Since ZACs have two oppositely charged moieties, the interactions between ions and varied ZACs would affect their surface scaling tendency.

To characterize the scale-forming ion adsorption capability of various types of ZAC coatings, the kinetic processes of calcium and sulfate salt adsorption on thin ZAC coatings (Figure S4) were investigated and compared. As shown in Figure 5A,B, the frequency (Δf) and dissipation (ΔD) during the initial 2 h period exhibited stable baselines. Once the introduction of calcium (Ca^{2+}, as $CaCl_2$) or sulfate (SO_4^{2-}, as Na_2SO_4) ion solution started, the frequency shift occurred rapidly, indicating the accumulation of ions on empty ZAC coatings (Figures S6 and S7). Compared to PT:MPC and PM:MPC, Δf of PT:SBMA and PM:SBMA in the presence of $CaCl_2$ or Na_2SO_4 decreased to the equilibrium state quicker; even the change rate was observed much more negligibly in the later stage. It was reported that Δf in the presence of salt solutions was closely related to the change in the amount of

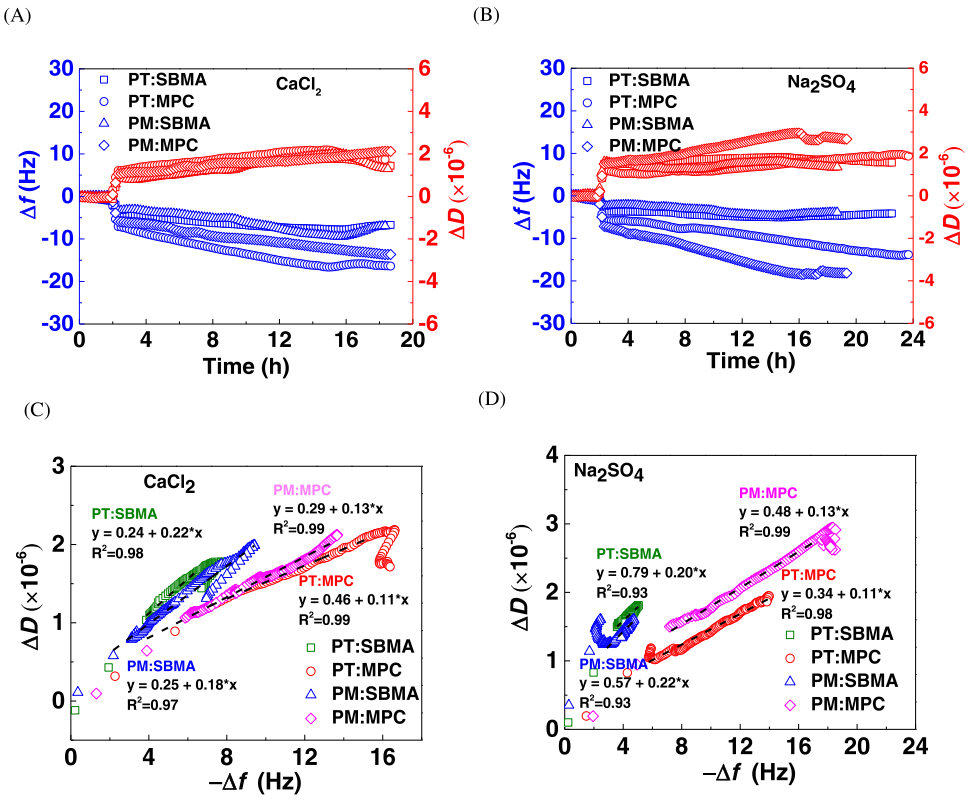

Figure 5. Changes of Δf and ΔD vs time at the third overtone during flowing 30 mM $CaCl_2$ (A) and 30 mM Na_2SO_4 (B) (note: the initial 2 h period refers to the stage of DI stabilization). ΔD vs Δf (D−f plot) at the third overtone for all ZACs during flowing $CaCl_2$(C) and Na_2SO_4 solution (D) through the QCM-D chamber (note: the linear trend line in the figure was fitted by Origin 9.0).

https://doi.org/10.1021/acsapm.2c01014
ACS Appl. Polym. Mater. 2022, 4, 7090−7101

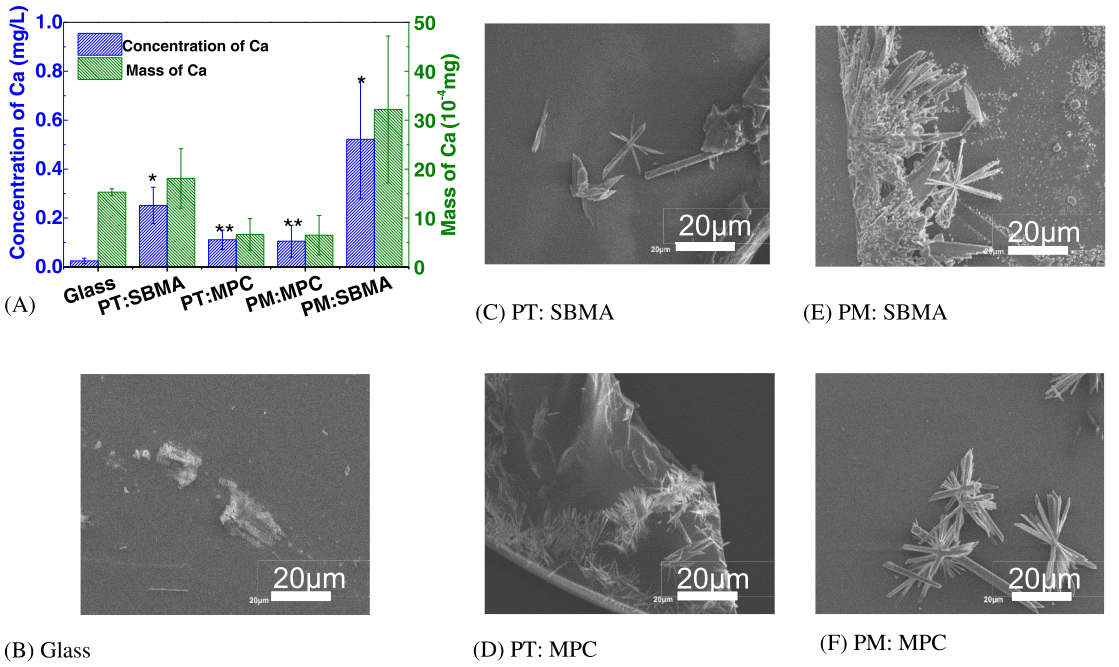

Figure 6. Concentration and mass of Ca measured by dissolving calcium sulfate precipitates formed on different substrates under a low SI (A) (note: * represents the statistically significant difference (p = 0.025 < 0.05) between PT:SBMA and PM:SBMA; **refers to the statistically insignificant difference (p = 0.94 > 0.05) between PT:MPC and PM:MPC); SEM images of heterogeneous calcium sulfate precipitates on (B) glass, (C) PT:SBMA, (D) PT:MPC, (E) PM:SBMA, and (F) PM:MPC. The scale bar is 20 μm.

the coupled water molecules inside the pSBMA polymer brushes induced by the solvation/desolvation of the grafted chains.[47] Therefore, due to the higher hydration capability of MPC functional groups, a relatively long time might be required to reach the balance between the solvation and desolvation, once the functional groups were paired with counterions.[48,49]

The change of dissipation (ΔD) in the presence of 30 mM $CaCl_2$ or 30 mM Na_2SO_4 mainly exhibited a monotonic increase, as shown in Figure 5A,B, which implied the increasing viscoelasticity of ZAC-coated sensor surfaces. To further reveal the detailed structural evolution of ZAC coatings during the flowing of $CaCl_2$ and Na_2SO_4 solutions, the relationship between ΔD and Δf before reaching the equilibrium state was analyzed, as shown in Figure 5C,D. In the presence of $CaCl_2$ (Figure 5C), ΔD for all ZAC coatings increased with the increasing Δf. Moreover, the linear and continuous trend between ΔD and Δf was obtained (R^2 > 0.95), which demonstrated little conformational change of ZAC-coated sensor surfaces upon flowing the $CaCl_2$ solution.[50] While in the presence of Na_2SO_4, a linear and continuous plot of ΔD against Δf (R^2 > 0.95) for ZAC coatings, except for PM:SBMA, was still observed in Figure 5D. In the initial stages, ΔD of PM:SBMA decreased with the increase of Δf with a negative slope, and the slope of ΔD against Δf shifted to a positive value at the later stage, which suggested that the conformation change or adjustment occurred upon flowing Na_2SO_4 over the PM:SBMA coating.

Based on the slope ($-\Delta D/\Delta f$) of the D–f plot and the method mentioned before, Δf and ΔD have been converted to the profile of mass changes, as shown in Figure S8A. Similar to the frequency change in the presence of $CaCl_2$ and Na_2SO_4, the slopes of mass change curves at the interval of 2–4 h for ZACs containing SBMA exhibited greater than those of ZACs containing MPC, indicating that SBMA polymers might have stronger ion adsorption capability in comparison to MPC polymers. Since the materials with less hydrophilicity (i.e., PT:SBMA/PM:SBMA) are likely to promote the adsorption of Ca–SO_4 ion pairs,[7] it might be the reason for such a difference in the ion adsorption kinetics. Moreover, the total mass changes under the equilibrium state were also quantified in Figure S8B. The total mass changes for PT:MPC and PM:MPC in the presence of $CaCl_2$ and Na_2SO_4 were greater than those of the PT:SBMA and PM:SBMA, respectively. Note that for each zwitterionic coating in Figure S8B, the total mass changes in the presence of $CaCl_2$ and Na_2SO_4 did not display a significant statistical difference, which might be related to zwitterion monomers with the same amount of cationic and anionic moieties.

3.3. Quantification of $CaSO_4$ Precipitates Formed under a Lower SI on ZAC Coatings. Figure 6A presents the concentration of Ca in the acidized solution in which $CaSO_4$ precipitates formed on different ZAC coatings under a low SI condition (SI = 0.07; Table 1) were dissolved for AAS measurements. Also, the mass of Ca in the acidized solution was calculated based on the concentration of Ca measured by AAS. The concentration and mass of Ca formed on ZAC coatings at the low SI value follow the order: PM:SBMA > PT:SBMA > PT:MPC ≅ PM:MPC. The differences in the concentration and mass of Ca between PT:MPC and PM:MPC (Student's t-test: p = 0.943 > 0.05) were not statistically significant. Both the concentration and mass of Ca for PT:MPC and PM:MPC were less than those of PT:SBMA and PM:SBMA, indicating that more precipitates formed on ZAC coatings containing SBMA than those containing MPC.

To further confirm the occurrence of heterogeneous precipitation on various types of ZAC coatings, the morphology of the precipitates was observed under SEM. As indicated in Figure 6C–F, the morphology of the precipitates on ZAC coatings exhibited the typical structure of gypsum

https://doi.org/10.1021/acsapm.2c01014
ACS Appl. Polym. Mater. 2022, 4, 7090–7101

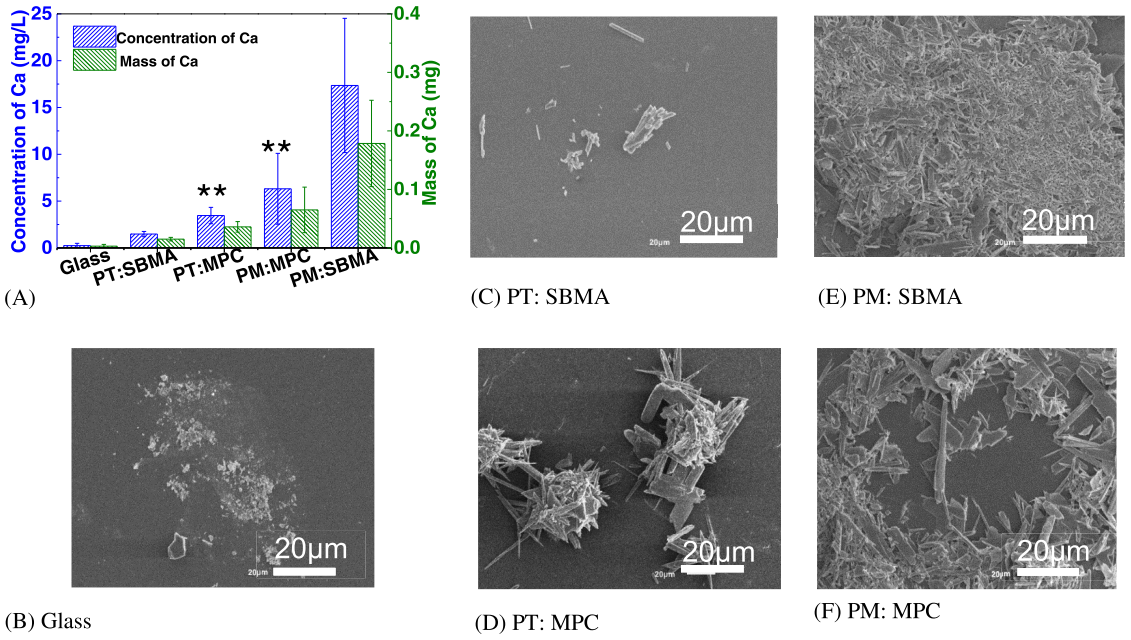

(A) (B) Glass (C) PT: SBMA (D) PT: MPC (E) PM: SBMA (F) PM: MPC

Figure 7. Concentration and mass of Ca in the acidized solution after the dissolution of $CaSO_4$ precipitates formed on different substrates under a high SI. (A) (**refers to the statistically insignificant difference (p = 0.22) between PT:MPC and PM:MPC). SEM images of homogeneous calcium sulfate precipitates and deposits on (B) glass, (C) PT:SBMA, (D) PT:MPC, (E) PM:SBMA, and (F) PM:MPC. The scale bar is 20 μm.

rosettes. Such a kind of shape was also observed on the polyamide membrane, which was attributed to surface-induced heterogeneous crystallization on membranes.[18] Besides, it can be seen from SEM images that the surface area covered by the scaling of PM:SBMA was larger than those of PM:MPC. Based on the quantification results and SEM images, ZAC coatings containing MPC had better-scaling-resistant performance than those coatings containing SBMA.

Based on the classical nucleation theory (Text S3), the trend of surface-induced crystallization for materials relies on the interfacial energy of the liquid−substrate that is associated with the surface hydrophilicity of the substrate.[39,51] Considering that, the detailed mechanisms may be explained as follows: first, the more hydrophilic the substrate is, the lower the interfacial energy of liquid−substrate, leading to a higher interfacial energy barrier and the unfavorable tendency for heterogeneous precipitation. Hence, the best scaling-resistant performance of MPC copolymer coating was ascribed to their relatively superior hydrophilicity to SBMA copolymer materials (Figure 2). Furthermore, the peaks corresponding to sulfobetaine and phosphate functional group of SBMA and MPC coatings after surface crystallization shifted obviously compared to before (Figure S9A,B), indicating that the ion adsorption (Ca^{2+} or SO_4^{2-}) may occur on the ZAC coating surfaces during the crystallization process. From this perspective, due to SBMA coatings' lower hydrophilicity, scale-forming ions can be rapidly adsorbed near SBMA coating surfaces in comparison with MPC coatings, which might change the local saturation indices at the substrate−liquid interface, thus accelerating $CaSO_4$ scaling kinetics on SBMA coatings. Additionally, the total mass changes for MPC coatings in the presence of $CaCl_2$ and Na_2SO_4 were greater than those of SBMA coatings, which, however, did not correlate with the amounts of precipitates formed on MPC coatings under low SI conditions. Therefore, compared to the mass changes, the adsorption kinetics of scale-forming ions to ZAC coatings played a more important role in controlling heterogeneous $CaSO_4$ precipitation.

3.4. Quantification of $CaSO_4$ Precipitates Formed under a Higher SI on ZAC Coatings. Similar to Figure 6A, the concentration of Ca in the acidized solution after the dissolution of $CaSO_4$ precipitates from different types of ZAC coatings is shown in Figure 7A. Also, the mass of Ca was calculated correspondingly using the concentration of Ca in the dissolution solution. With the increasing SI value (SI = 0.32; Table 1), the deposition/adhesion of crystals formed in bulk solution would be dominated. The order of concentration and mass of Ca after dissolving the deposited $CaSO_4$ on varied ZAC coatings were the following: PT:SBMA < PT:MPC ≅ PM:MPC < PM:SBMA. This indicates that the least and most precipitates occurred on the PT:SBMA and PM:SBMA coatings, respectively, while the precipitated masses on both PT:MPC and PM:MPC displayed no significantly statistical difference (p = 0.22 > 0.05). The quantification results were further corroborated by SEM characterizations. In Figure 7B−F, the surface coverage by scaling for ZACs containing MMA hydrophobic units appeared to be greater than that for ZACs containing TFEMA hydrophobic units. Also, SEM images displayed plate-like and needle-like crystals on various ZAC coatings, confirming that $CaSO_4$ precipitates were formed under a high SI condition through the deposition of homogeneous precipitates. From the precipitate quantification results and SEM observations, it can be concluded that ZAC coatings containing TFEMA hydrophobic units performed better in scaling resistance than those containing MMA hydrophobic units. The difference in the scaling-resistant performance of ZAC coatings might be associated with the hydrophobic unit of the ZAC coatings. Among all ZAC coatings, PT:SBMA displayed the best scaling resistance compared to the other three.

Hydrophobic or superhydrophobic surfaces are known to improve the surface antiscaling efficiency as hydrophobic materials with lower surface energy could inhibit scaling

https://doi.org/10.1021/acsapm.2c01014
ACS Appl. Polym. Mater. 2022, 4, 7090−7101

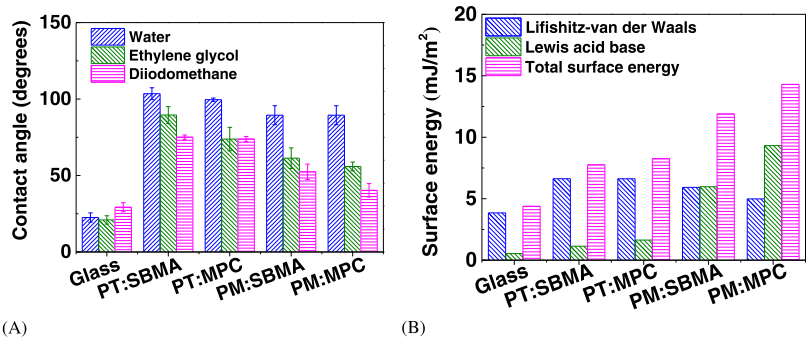

Figure 8. (A) Contact angles measured with water, ethylene glycol, and diiodomethane; and (B) surface energy of various ZAC coatings including Lifshitz−van der Waals and Lewis acid−base components.

Table 3. Comparison Results of the Interfacial Energy, Surface Charge, and Roughness[a]

	ΔG_{nls}^{T}	ΔG_{nls}^{Lw}	ΔG_{nls}^{AB}	ζ potential (pH = 6) (mv)	roughness (Rq/nm)
PT:SBMA	−22.9	9.2	−32.1	NA	8.27 ± 1.95
PT:MPC	−23.2	9.2	−32.4	−17.2 ± 0.2	9.81 ± 1.72
PM:SBMA	−9.0	9.8	−18.8	−23.0 ± 0.6	27.23 ± 0.21
PM:MPC	−4.7	10.7	−15.4	−17.1 ± 0.3	24.28 ± 1.90

[a]NA refers to not detected.

deposition and even bacterial adhesion.[15,52−55] In contrast, the hydrophilic surfaces with higher surface energy can alleviate protein or mineral nucleation due to the larger polar components.[7,23,56,57] Therefore, to determine $CaSO_4$ scaling mechanisms on ZAC coatings, we first measured the Lifshitz−van der Waals and Lewis acid−base components of ZAC coatings' total surface energy using three probe liquids.[15,58] The polar (Lewis acid−base) and nonpolar (Lifshitz−van der Waals) components are calculated by the three liquid probe measurements (Table S2). The specific calculation details can be referenced in the supporting material (Text S2 and Tables S1 and S2).

Figure 8A,B shows the contact angles of three liquid probes, the surface energy, and their corresponding surface tension components. In Figure 8A, water contact angles >90° for four types of ZAC coatings confirmed their hydrophobic properties. And the order of the total surface energy in Figure 8B is PM:MPC > PM:SBMA > PT:MPC > PT:SBMA. Here, PT:SBMA with the lowest surface energy could reduce the deposition/adsorption of $CaSO_4$ precipitates, thus rendering the least amount of precipitates formed on their coating surfaces. The surface energy of ZAC coatings containing TFEMA hydrophobic units (i.e., PT:SBMA and PT:MPC) was lower than those of ZAC coatings containing MMA hydrophobic units (i.e., PM:SBMA and PM:MPC), which might explain why PT:SBMA and PT:MPC had fewer precipitates than PM:SBMA and PM:MPC. The low surface energy of PT:SBMA and PT:MPC was because the fluorine atoms in TFEMA have a full octet of electrons, which could reduce the surface polarity and, in turn, lower their relatively Lewis acid-based energy.[15] For PM:SBMA and PM:MPC, it was found that the amounts of precipitates are inconsistent with their surface energies. According to Van Oss et al., surface energy is regarded as the description of thermodynamic surface equilibrium in a vacuum.[59] Since the scaling process actually relies on the mutual interactions among the crystal, the substrate, and the liquid, we hypothesized that the total interaction energy could explain such inconsistency for PM:SBMA and PM:MPC.

Based on the extended Derjaguin−Landau−Verwey−Overbeek (x-DLVO) theory, the total interaction energy ΔG_{nls}^{T} consists of the Lifshitz−van der Waals (LW) forces, acid−base (AB) forces, and the electrostatic double-layer (EL) forces.[34,59] The electrostatic double-layer force was usually neglected in prior studies due to its relatively low value compared to the other two types of interaction forces.[34,60] Therefore, it will not be considered in the following total interaction energy calculation. By referencing previously reported surface tension components of $CaSO_4$ crystals and water,[7,61] the total interfacial energy (ΔG_{nls}^{T}) among the precipitates, water, and ZAC coatings was calculated using the formula

$$\begin{aligned}\Delta G_{nls}^{T} &= \Delta G_{nls}^{Lw} + \Delta G_{nls}^{AB} \\ &= 2[(\sqrt{\gamma_n^{Lw}\gamma_l^{Lw}} + \sqrt{\gamma_s^{Lw}\gamma_l^{Lw}} - \sqrt{\gamma_n^{Lw}\gamma_s^{Lw}} - \gamma_l^{Lw}) \\ &\quad + \sqrt{\gamma_l^{+}}(\sqrt{\gamma_n^{-}} + \sqrt{\gamma_s^{-}} - \sqrt{\gamma_l^{-}}) \\ &\quad + \sqrt{\gamma_l^{-}}(\sqrt{\gamma_n^{+}} + \sqrt{\gamma_s^{+}} - \sqrt{\gamma_l^{+}}) - \sqrt{\gamma_n^{+}\gamma_s^{-}} \\ &\quad - \sqrt{\gamma_n^{-}\gamma_s^{+}}]\end{aligned} \tag{2}$$

where n, s, and l represent the precipitates, substrate, and liquid, respectively; and γ^{LW}, γ^{AB}, γ^{+}, and γ^{-} are different components of the surface tension of the material. More detailed descriptions of the x-DLVO model are presented in the Supporting Information (Text S4).

As shown in Table 3, the total interaction energies ΔG_{nls}^{T} between $CaSO_4$ and PT:SBMA, PT:MPC, PM:SBMA, and PM:MPC coatings were calculated as −22.9, −23.2, −9.0, and −4.7 mJ m^{-2}, respectively, which represented the attractive interactions between precipitates and ZAC coatings. Given that the more negative the total interaction energy was, the more favorable the scaling tendency would be.[55] As the total interaction energy for PM:MPC was higher (less negative) than that of PM:SBMA, it was expected that fewer precipitates formed on PM:MPC coatings than on PM:SBMA. The same interpretation was also applied for the lower quantity of

https://doi.org/10.1021/acsapm.2c01014
ACS Appl. Polym. Mater. 2022, 4, 7090−7101

precipitates on PT:SBMA coatings because their values of ΔG_{nls}^{T} are less negative than that of PT:MPC coatings.

Other than the effect of thermodynamic equilibrium, the deposition affinity of homogeneous precipitates was also affected by the surface roughness. As aforementioned, the average surface roughness for PT:MPC and PT:SBMA exhibited no significant statistical difference (Figure 3 and Table 3). For both PM:SBMA and PM:MPC, the average surface roughness was higher than those of both PT:SBMA and PT:MPC, thus causing more contact sites for the scaling deposition. Moreover, such morphological heterogeneities for PM:MPC and PM:SBMA might result in higher (less negative) total interaction energies compared to both PT:MPC and PT:SBMA, as a rougher surface can reduce the magnitude of the interaction energy.[34,62,63] Hence, it can be suggested that the surface roughness caused the discrepancy between the true scaling behaviors and the theoretical x-DLVO prediction value. To summarize, the total interaction energy calculated based on x-DLVO theory alone might not be able to explain the true scaling behaviors well. Together with it, the presence of the surface chemical (i.e., charge density) or morphological (i.e., roughness) heterogeneities that can affect the surface energy distribution should also be considered.

4. CONCLUSIONS

Various ZACs were synthesized from different zwitterion monomers (i.e., SBMA and MPC) and hydrophobic monomers (TFEMA and MMA) using FRP to study their scaling-resistant performance and the underlying scaling mechanisms. Batch $CaSO_4$ scaling tests on different types of ZAC-coated substrates were conducted under lower or higher SI conditions. For homogeneous precipitation under a higher SI condition (SI_{gyp} = 0.32), fewer $CaSO_4$ precipitates occurred on ZAC coatings containing TFEMA hydrophobic units compared to those ZAC coatings containing MMA hydrophobic units because of the lower surface energy of TFEMA copolymer coatings. In addition, PT:SBMA exhibited a smooth surface with the lowest surface energy, which inhibited the crystal adsorption/deposition better than the other three types of ZAC coatings. For the heterogeneous precipitation of $CaSO_4$, under a lower SI condition (SI_{gyp} = 0.07), ZAC coatings containing MPC showed better-scaling resistance than those containing SBMA. This was due to the less hydrophilic ZAC coatings containing SBMA being more prone to scale-forming ion adsorption, thus increasing the saturation level near the local coating surface and promoting the scaling kinetic rate on these coatings compared to ZACs containing MPC. Even so, further research studies on how ZAC coatings specifically affect the kinetic rate of heterogeneous $CaSO_4$ precipitation, especially for the nucleation and growth stage, still need to be explored. In summary, these findings can help to understand the fundamental mechanisms of ZACs controlling mineral scaling. To design antiscaling coatings or selective layer materials, ZAC coatings with higher hydrophilicity and lower roughness can be good candidates.

ASSOCIATED CONTENT

Supporting Information

The Supporting Information is available free of charge at https://pubs.acs.org/doi/10.1021/acsapm.2c01014.

The Supporting Information includes the ZAC synthesis protocols, the surface energy tension component calculation based on the three probe liquids, and the interfacial energy calculation based on the x-DLVO theory (PDF)

(PDF)

AUTHOR INFORMATION

Corresponding Author

Debora F. Rodrigues − *Department of Civil & Environmental Engineering, University of Houston, Houston, Texas 77004, United States;* orcid.org/0000-0002-3124-1443; Phone: 713-743-1495; Email: dfrigirodrigues@uh.edu.; Fax: 713-743-4260

Authors

Meng Wang − *Department of Civil & Environmental Engineering, University of Houston, Houston, Texas 77004, United States*

Hoang Nguyen − *Department of Civil & Environmental Engineering, University of Houston, Houston, Texas 77004, United States*

Samuel J. Lounder − *Department of Chemical and Biological Engineering, Tufts University, Medford, Massachusetts 02155, United States*

Ayse Asatekin − *Department of Chemical and Biological Engineering, Tufts University, Medford, Massachusetts 02155, United States;* orcid.org/0000-0002-4704-1542

Complete contact information is available at: https://pubs.acs.org/10.1021/acsapm.2c01014

Notes

The authors declare no competing financial interest.

ACKNOWLEDGMENTS

The authors would like to thank the funding support from National Science Foundation (grant no. CHE-1904472). The authors also appreciate Dr. Devin Shaffer and Pablo Bribiesca for their assistance in the measurements of the surface streaming ζ potential.

REFERENCES

(1) Tong, T.; Wallace, A. F.; Zhao, S.; Wang, Z. Mineral Scaling in Membrane Desalination: Mechanisms, Mitigation Strategies, and Feasibility of Scaling-Resistant Membranes. *J. Membr. Sci.* **2019**, *579*, 52−69.

(2) Mady, M. F.; Kelland, M. A. Review of Nanotechnology Impacts on Oilfield Scale Management. *ACS Appl. Nano Mater.* **2020**, *3*, 7343−7364.

(3) Karanikola, V.; Boo, C.; Rolf, J.; Elimelech, M. Engineered Slippery Surface to Mitigate Gypsum Scaling in Membrane Distillation for Treatment of Hypersaline Industrial Wastewaters. *Environ. Sci. Technol.* **2018**, *52*, 14362−14370.

(4) Mauermann, M.; Eschenhagen, U.; Bley, T.; Majschak, J. P. Surface Modifications − Application Potential for the Reduction of Cleaning Costs in the Food Processing Industry. *Trends Food Sci. Technol.* **2009**, *20*, S9−S15.

(5) Antony, A.; Low, J. H.; Gray, S.; Childress, A. E.; Le-Clech, P.; Leslie, G. Scale Formation and Control in High Pressure Membrane Water Treatment Systems: A Review. *J. Membr. Sci.* **2011**, *383*, 1−16.

(6) Chen, S. C.; Su, J.; Fu, F.-J.; Mi, B.; Chung, T.-S. Gypsum ($CaSO_4{\cdot}2H_2O$) Scaling on Polybenzimidazole and Cellulose Acetate Hollow Fiber Membranes under Forward Osmosis. *Membranes* **2013**, *3*, 354−374.

(7) Huang, X.; Li, C.; Zuo, K.; Li, Q. Predominant Effect of Material Surface Hydrophobicity on Gypsum Scale Formation. *Environ. Sci. Technol.* **2020**, *54*, 15395−15404.
(8) Qi, Y.; Tong, T.; Zhao, S.; Zhang, W.; Wang, Z.; Wang, J. Reverse Osmosis Membrane with Simultaneous Fouling- and Scaling-Resistance Based on Multilayered Metal-Phytic Acid Assembly. *J. Membr. Sci.* **2020**, *601*, No. 117888.
(9) Lyster, E.; Kim, M. man.; Au, J.; Cohen, Y. A Method for Evaluating Antiscalant Retardation of Crystal Nucleation and Growth on RO Membranes. *J. Membr. Sci.* **2010**, *364*, 122−131.
(10) Shih, W. Y.; Gao, J.; Rahardianto, A.; Glater, J.; Cohen, Y.; Gabelich, C. J. Ranking of Antiscalant Performance for Gypsum Scale Suppression in the Presence of Residual Aluminum. *Desalination* **2006**, *196*, 280−292.
(11) Mangal, M. N.; Salinas-Rodriguez, S. G.; Dusseldorp, J.; Kemperman, A. J. B.; Schippers, J. C.; Kennedy, M. D.; van der Meer, W. G. J. Effectiveness of Antiscalants in Preventing Calcium Phosphate Scaling in Reverse Osmosis Applications. *J. Membr. Sci.* **2021**, *623*, No. 119090.
(12) Zhou, C.; Ye, D.; Jia, H.; Yu, S.; Liu, M.; Gao, C. Surface Mineralization of Commercial Thin-Film Composite Polyamide Membrane by Depositing Barium Sulfate for Improved Reverse Osmosis Performance and Antifouling Property. *Desalination* **2014**, *351*, 228−235.
(13) Huang, Y.-X.; Liang, D.; Luo, C.; Zhang, Y.; Meng, F. Liquid-like Surface Modification for Effective Anti-Scaling Membrane Distillation with Uncompromised Flux. *J. Membr. Sci.* **2021**, *637*, No. 119673.
(14) Ansari, A.; Peña-Bahamonde, J.; Wang, M.; Shaffer, D. L.; Hu, Y.; Rodrigues, D. F. Polyacrylic Acid-Brushes Tethered to Graphene Oxide Membrane Coating for Scaling and Biofouling Mitigation on Reverse Osmosis Membranes. *J. Membr. Sci.* **2021**, *630*, No. 119308.
(15) Sojoudi, H.; Nemani, S. K.; Mullin, K. M.; Wilson, M. G.; Aladwani, H.; Lababidi, H.; Gleason, K. K. Micro-/Nanoscale Approach for Studying Scale Formation and Developing Scale-Resistant Surfaces. *ACS Appl. Mater. Interfaces* **2019**, *11*, 7330−7337.
(16) Guan, Y. F.; Boo, C.; Lu, X.; Zhou, X.; Yu, H. Q.; Elimelech, M. Surface Functionalization of Reverse Osmosis Membranes with Sulfonic Groups for Simultaneous Mitigation of Silica Scaling and Organic Fouling. *Water Res.* **2020**, *185*, No. 116203.
(17) Mi, B.; Elimelech, M. Gypsum Scaling and Cleaning in Forward Osmosis: Measurements and Mechanisms. *Environ. Sci. Technol.* **2010**, *44*, 2022−2028.
(18) Shaffer, D. L.; Tousley, M. E.; Elimelech, M. Influence of Polyamide Membrane Surface Chemistry on Gypsum Scaling Behavior. *J. Membr. Sci.* **2017**, *525*, 249−256.
(19) Hamm, L. M.; Giuffre, A. J.; Han, N.; Tao, J.; Wang, D.; De Yoreo, J. J.; Dove, P. M. Reconciling Disparate Views of Template-Directed Nucleation through Measurement of Calcite Nucleation Kinetics and Binding Energies. *Proc. Natl. Acad. Sci. U.S.A.* **2014**, *111*, 1304−1309.
(20) Giuffre, A. J.; Hamm, L. M.; Han, N.; De Yoreo, J. J.; Dove, P. M. Polysaccharide Chemistry Regulates Kinetics of Calcite Nucleation through Competition of Interfacial Energies. *Proc. Natl. Acad. Sci. U.S.A.* **2013**, *110*, 9261−9266.
(21) Smeets, P. J. M.; Cho, K. R.; Kempen, R. G. E.; Sommerdijk, N. A. J. M.; Yoreo, J. J. De. Calcium Carbonate Nucleation Driven by Ion Binding in a Biomimetic Matrix Revealed by in Situ Electron Microscopy. *Nat. Mater.* **2015**, *14*, 394−399.
(22) Deng, N.; Stack, A. G.; Weber, J.; Cao, B.; De Yoreo, J. J.; Hu, Y. Organic−Mineral Interfacial Chemistry Drives Heterogeneous Nucleation of Sr-Rich $(Ba_x, Sr_{1-x})SO_4$ from Undersaturated Solution. *Proc. Natl. Acad. Sci. U.S.A.* **2019**, *116*, 13221−13226.
(23) Jaramillo, H.; Boo, C.; Hashmi, S. M.; Elimelech, M. Zwitterionic Coating on Thin-Film Composite Membranes to Delay Gypsum Scaling in Reverse Osmosis. *J. Membr. Sci.* **2021**, *618*, No. 118568.
(24) Ray, J. R.; Wong, W.; Jun, Y.-S. Antiscaling Efficacy of $CaCO_3$ and $CaSO_4$ on Polyethylene Glycol (PEG)-Modified Reverse Osmosis Membranes in the Presence of Humic Acid: Interplay of Membrane Surface Properties and Water Chemistry. *Phys. Chem. Chem. Phys* **2017**, *19*, 5647−5657.
(25) Zheng, J.; He, Y.; Chen, S.; Li, L.; Bernards, M. T.; Jiang, S. Molecular Simulation Studies of the Structure of Phosphorylcholine Self-Assembled Monolayers. *J. Chem. Phys.* **2006**, *125*, No. 174714.
(26) Shao, Q.; He, Y.; White, A. D.; Jiang, S. Difference in Hydration between Carboxybetaine and Sulfobetaine. *J. Phys. Chem. B* **2010**, *114*, 16625−16631.
(27) Bengani-Lutz, P.; Converse, E.; Cebe, P.; Asatekin, A. Self-Assembling Zwitterionic Copolymers as Membrane Selective Layers with Excellent Fouling Resistance: Effect of Zwitterion Chemistry. *ACS Appl. Mater. Interfaces* **2017**, *9*, 20859−20872.
(28) Bengani-Lutz, P.; Zaf, R. D.; Culfaz-Emecen, P. Z.; Asatekin, A. Extremely Fouling Resistant Zwitterionic Copolymer Membranes with ∼ 1 Nm Pore Size for Treating Municipal, Oily and Textile Wastewater Streams. *J. Membr. Sci.* **2017**, *543*, 184−194.
(29) Dudchenko, A. V.; Bengani-Lutz, P.; Asatekin, A.; Mauter, M. S. Foulant Adsorption to Heterogeneous Surfaces with Zwitterionic Nanoscale Domains. *ACS Appl. Polym. Mater.* **2020**, *2*, 4709−4718.
(30) Ozcan, S.; Kaner, P.; Thomas, D.; Cebe, P.; Asatekin, A. Hydrophobic Antifouling Electrospun Mats from Zwitterionic Amphiphilic Copolymers. *ACS Appl. Mater. Interfaces* **2018**, *10*, 18300−18309.
(31) Dai, C.; Zhao, J.; Giammar, D. E.; Pasteris, J. D.; Zuo, X.; Hu, Y. Heterogeneous Lead Phosphate Nucleation at Organic-Water Interfaces: Implications for Lead Immobilization. *ACS Earth Space Chem.* **2018**, *2*, 869−877.
(32) Dai, C.; Stack, A. G.; Koishi, A.; Fernandez-Martinez, A.; Lee, S. S.; Hu, Y. Heterogeneous Nucleation and Growth of Barium Sulfate at Organic-Water Interfaces: Interplay between Surface Hydrophobicity and Ba^{2+} Adsorption. *Langmuir* **2016**, *32*, 5277−5284.
(33) Azimi, G.; Cui, Y.; Sabanska, A.; Varanasi, K. K. Scale-Resistant Surfaces: Fundamental Studies of the Effect of Surface Energy on Reducing Scale Formation. *Appl. Surf. Sci.* **2014**, *313*, 591−599.
(34) Brant, J. A.; Childress, A. E. Assessing Short-Range Membrane-Colloid Interactions Using Surface Energetics. *J. Membr. Sci.* **2002**, *203*, 257−273.
(35) Xie, M.; Gray, S. R. Gypsum Scaling in Forward Osmosis: Role of Membrane Surface Chemistry. *J. Membr. Sci.* **2016**, *513*, 250−259.
(36) Han, L.; Tan, Y. Z.; Xu, C.; Xiao, T.; Trinh, T. A.; Chew, J. W. Zwitterionic Grafting of Sulfobetaine Methacrylate (SBMA) on Hydrophobic PVDF Membranes for Enhanced Anti-Fouling and Anti-Wetting in the Membrane Distillation of Oil Emulsions. *J. Membr. Sci.* **2019**, *588*, No. 117196.
(37) McCool, B. C.; Rahardianto, A.; Faria, J. I.; Cohen, Y. Evaluation of Chemically-Enhanced Seeded Precipitation of RO Concentrate for High Recovery Desalting of High Salinity Brackish Water. *Desalination* **2013**, *317*, 116−126.
(38) McCool, B. C.; Rahardianto, A.; Faria, J.; Kovac, K.; Lara, D.; Cohen, Y. Feasibility of Reverse Osmosis Desalination of Brackish Agricultural Drainage Water in the San Joaquin Valley. *Desalination* **2010**, *261*, 240−250.
(39) Cao, B.; Ansari, A.; Yi, X.; Rodrigues, D. F.; Hu, Y. Gypsum Scale Formation on Graphene Oxide Modified Reverse Osmosis Membrane. *J. Membr. Sci.* **2018**, *552*, 132−143.
(40) Wang, M.; Cao, B.; Hu, Y.; Rodrigues, D. F. Mineral Scaling on Reverse Osmosis Membranes: Role of Mass, Orientation, and Crystallinity on Permeability. *Environ. Sci. Technol.* **2021**, *55*, 16110−16119.
(41) Meléndrez, D.; Jowitt, T.; Iliut, M.; Verre, A. F.; Goodwin, S.; Vijayaraghavan, A. Adsorption and Binding Dynamics of Graphene-Supported Phospholipid Membranes Using the QCM-D Technique. *Nanoscale* **2018**, *10*, 2555−2567.
(42) Lapidot, T.; Sedransk Campbell, K. L.; Heng, J. Y. Y. Model for Interpreting Surface Crystallization Using Quartz Crystal Microbalance: Theory and Experiments. *Anal. Chem.* **2016**, *88*, 4886−4893.

https://doi.org/10.1021/acsapm.2c01014
ACS Appl. Polym. Mater. 2022, 4, 7090−7101

(43) Cho, N. J.; Frank, C. W.; Kasemo, B.; Höök, F. Quartz Crystal Microbalance with Dissipation Monitoring of Supported Lipid Bilayers on Various Substrates. *Nat. Protoc.* **2010**, *5*, 1096−1106.
(44) Li, D.; Wei, Q.; Wu, C.; Zhang, X.; Xue, Q.; Zheng, T.; Cao, M. Superhydrophilicity and Strong Salt-Affinity: Zwitterionic Polymer Grafted Surfaces with Significant Potentials Particularly in Biological Systems. *Adv. Colloid Interface Sci.* **2020**, *278*, No. 102141.
(45) Lu, X.; Zhang, C.; Cui, X.; Zhu, T.; Zong, M.Nucleation and Growth of Crystal on a Substrate Surface: Structure Matching at the Atomistic Level. In *Crystallization via Nonclassical Pathways Volume 1: Nucleation, Assembly, Observation & Application*, ACS Symposium Series; American Chemical Society, 2020; Vol. *1358*, pp 295−310.
(46) Dai, C.; Zuo, X.; Cao, B.; Hu, Y. Homogeneous and Heterogeneous (Fex, Cr1-x)(OH)3 Precipitation: Implications for Cr Sequestration. *Environ. Sci. Technol.* **2016**, *50*, 1741−1749.
(47) Wang, T.; Wang, X.; Long, Y.; Liu, G.; Zhang, G. Ion-Specific Conformational Behavior of Polyzwitterionic Brushes: Exploiting It for Protein Adsorption/Desorption Control. *Langmuir* **2013**, *29*, 6588−6596.
(48) Shao, Q.; Mi, L.; Han, X.; Bai, T.; Liu, S.; Li, Y.; Jiang, S. Differences in Cationic and Anionic Charge Densities Dictate Zwitterionic Associations and Stimuli Responses. *J. Phys. Chem. B* **2014**, *118*, 6956−6962.
(49) Zhang, Z.; Moxey, M.; Alswieleh, A.; Morse, A. J.; Lewis, A. L.; Geoghegan, M.; Leggett, G. J. Effect of Salt on Phosphorylcholine-Based Zwitterionic Polymer Brushes. *Langmuir* **2016**, *32*, 5048−5057.
(50) Kawelah, M.; He, Y.; Alamri, H.; Gizzatov, A.; Swager, T. M.; Zhu, S. S. Dynamic Adsorption of Functionalized Zwitterionic Copolymers on Carbonate Surfaces under Extreme Reservoir Conditions. *Energy Fuels* **2020**, *34*, 12018−12025.
(51) Hu, Y.; Neil, C.; Lee, B.; Jun, Y. S. Control of Heterogeneous Fe(III) (Hydr)Oxide Nucleation and Growth by Interfacial Energies and Local Saturations. *Environ. Sci. Technol.* **2013**, *47*, 9198−9206.
(52) Guo, H.; Chen, P.; Tian, S.; Ma, Y.; Li, Q.; Wen, C.; Yang, J.; Zhang, L. Amphiphilic Marine Antifouling Coatings Based on Hydrophilic Polyvinylpyrrolidone and a Hydrophobic Fluorine−Silicon-Containing Block Copolymer. *Langmuir* **2020**, *36*, 14573−14581.
(53) Hadidi, M.; Zydney, A. L. Fouling Behavior of Zwitterionic Membranes: Impact of Electrostatic and Hydrophobic Interactions. *J. Membr. Sci.* **2014**, *452*, 97−103.
(54) Zhao, Q.; Liu, Y.; Wang, C.; Wang, S.; Müller-Steinhagen, H. Effect of Surface Free Energy on the Adhesion of Biofouling and Crystalline Fouling. *Chem. Eng. Sci.* **2005**, *60*, 4858−4865.
(55) Su, M.; Bai, Y.; Han, J.; Chen, J.; Sun, H. Adhesion of Gypsum Crystals to Polymer Membranes: Mechanisms and Prediction. *J. Membr. Sci.* **2018**, *566*, 104−111.
(56) Hao, Z.; Zhao, S.; Li, Q.; Wang, Y.; Zhang, J.; Wang, Z.; Wang, J. Reverse Osmosis Membranes with Sulfonate and Phosphate Groups Having Excellent Anti- Scaling and Anti-Fouling Properties. *Desalination* **2021**, *509*, No. 115076.
(57) Rahimi, A.; Stafslien, S. J.; Vanderwal, L.; Bahr, J.; Safaripour, M.; Finlay, J. A.; Clare, A. S.; Webster, D. C. Critical Amphiphilic Concentration: Effect of the Extent of Amphiphilicity on Marine Fouling-Release Performance. *Langmuir* **2021**, *37*, 2728−2739.
(58) Subhi, N.; Verliefde, A. R. D.; Chen, V.; Le-Clech, P. Assessment of Physicochemical Interactions in Hollow Fibre Ultrafiltration Membrane by Contact Angle Analysis. *J. Membr. Sci.* **2012**, *403*−*404*, 32−40.
(59) Van Oss, C. J. Acid—base interfacial interactions in aqueous media. *Colloids Surf., A* **1993**, *78*, 1−49.
(60) Zhang, S.; Ly, Q. V.; Nghiem, L. D.; Wang, J.; Li, J.; Hu, Y. Optimization and Organic Fouling Behavior of Zwitterion-Modified Thin-Film Composite Polyamide Membrane for Water Reclamation: A Comprehensive Study. *J. Membr. Sci.* **2020**, *596*, No. 117748.
(61) Teng, F.; Zeng, H.; Liu, Q. Understanding the Deposition and Surface Interactions of Gypsum. *J. Phys. Chem. C* **2011**, *115*, 17485−17494.
(62) Bhattacharjee, S.; Ko, C.-H.; Elimelech, M. DLVO Interaction between Rough Surfaces. *Langmuir* **1998**, *14*, 3365−3375.
(63) Walz, J. Y. The Effect of Surface Heterogeneities on Colloidal Forces. *Adv. Colloid Interface Sci.* **1998**, *74*, 119−168.

https://doi.org/10.1021/acsapm.2c01014
ACS Appl. Polym. Mater. 2022, 4, 7090−7101